Statistical Characterization of Shallow-Water Bistatic Sonar Reverberation and Noise

Kenneth D. Pack, Michael V. Turner, Dr. James M. Ling

TRW Systems Integration Group, One Federal Systems Park Dr., Fairfax, VA 22033, USA

Joseph M. Monti

Naval Undersea Warfare Center, Detachment New London, New London, CT 06320-5594, USA

Abstract Shallow-water, low-frequency bistatic sonar measurements often exhibit high noise caused by bathymetric reverberation and other sources. Understanding the noise statistics is an essential first step in developing filters that separate noise clutter from desired signals. This paper characterizes matched filter outputs from a bistatic receiver for a shallow-water environment for several waveforms. Data dominated by ambient noise are compared to reverberation from identifiable bathymetric returns. The direct blast reverberation tail is excluded. The measurements include various types of envelope time series power and power-spectral statistics. This analysis shows that ambient noise can be approximately explained using synthetic noise. Bathymetric returns have different statistics and are not predictable by synthetic noise.

1. Introduction

Research for next generation sonars has made some progress in characterizing the statistics of noise for a variety of sonar bands. Statistics that describe the shape of matched filter threshold crossing peaks or peak clusters have been developed. Such statistics can be used to construct filters that can separate the data into different classes based on the statistic's cumulative distribution function (CDF). Figure 1 shows how a thresholding filter can be constructed. While some work to establish the CDFs for deep water exists, little has been done to describe the same statistics for shallow water.

The data processed for this investigation were collected using a towed array as a bistatic receiver as shown in Figure 2. Data were collected south of Sicily on the Medina Bank.

This work is sponsored by the Office of Naval Research.

Two transmission periods of two hours each were available. The start of the second period is two hours after the end of the first. During the first period, the towed array receiver was in a water depth of approximately 280 m. During the second, the water depth under the receiver ranged from about 300 to 430 m. The water depth under the bistatic source for both periods was about 365 m.

The Medina ridge is a large, prominent, and well-mapped bathymetric feature. Bathymetric features are clustered to one side of the array, with the deep Ionian Basin to the other side. The geometry of this experiment suggested that bathymetric returns would be common and identifiable with mapped features.

The transmission schedule used in this experiment was the 20-minute multiscale keying scheme shown in Figure 3. There were four wavetrains (WT) in the scheme, two of which were outside the band processed. Waveforms consisted of hyperbolic frequency modulated (HFM), frequency shift keying (FSK), and pulsed continuous wave (CW) signals. CW was not processed for this analysis. The HFM was generated using:

$$f(t) = \sin\left(2\pi \frac{-f_s f_e T}{W} \ln\left(1 - \frac{Wt}{f_e T}\right)\right) \qquad (1)$$

where f_s is the starting frequency in the waveform,
f_e is the end frequency in the waveform,
W is the bandwidth of the waveform ($W = | f_s - f_e |$), and
T is the duration of the waveform.
Parameters used in the test may be accurately read from the figure.

The FSKs were generated using the COSTAS chip map shown in Table 1. The FSKs are identical except that their center frequencies are shifted by 80 Hz.

Wavetrain crosstalk is a consideration in a multiscale keying transmission. In wavetrains WT1 and WT3, the order of the HFM and FSK waveforms and the sub-bands to which they are assigned is reversed. This minimizes waveform crosstalk in the processing. While wavetrains WT2 and WT4 are out of band, they contribute to the noise, especially when their direct blast arrives at the towed array.

The objective of this research is to characterize some statistical measures that have been studied in deep water to a shallow water environment. The objective includes separation of noise into identifiable regions. These are the direct blast reverberation tail, bathymetric returns, and ambient noise. The last also may contain background reverberation. The dependence of a statistic on threshold and waveform used to calculate it is also to be determined.

2. Methods

This research consisted of signal processing followed by statistical analysis. Signal processing used TRW's 32-beam Multistatic Processing System (MPS) to do the processing shown in Figure 4 in three main parts. In the first part, data from the towed array are heterodyned to base band. Data are filtered to a 256 Hz bandwidth and decimated. Optionally, they are stored on tape.

In the second signal processing part, the same data are then processed on two parallel paths. HFM and FSK waveforms have independent paths.

In the second processing step on the HFM path, data are first replica correlated and detected. The matched filter output is range normalized to compute an estimate of the signal-to-noise ratio (SNR). A threshold test is used to identify significant threshold crossings. Threshold crossings are clustered by range and beam to remove redundant information from the output data.

In the third processing step for the HFM path, the threshold test is used to initiate the computation of statistics on the unnormalized matched filter output data. When threshold crossing data are combined, clusters are assigned statistics based on the strongest threshold crossing in the cluster. The clusters themselves also have statistics computed based on the normalized members of the clusters.

The second processing step for the FSK processing path is similar to the HFM path. Data are first processed using a matched CW filter. The output spectra are range normalized, and the SNR is computed for each spectral cell. Data are combined by post-detection pulse compression (PDPC) integration. Finally, data are clustered over range, Doppler, and beam.

The third processing step for FSK is computation of statistics. This also has a PDPC integration step. Here, the unnormalized data are summed, and the statistics for the peaks identified on the detection path are computed. As for HFM, the statistics of the strongest peak in a cluster are associated with the cluster. Also, statistics are computed for the cluster as a whole based on member threshold crossing SNRs.

Finally, data are passed on for statistical analysis. Data are optionally written to tape.

This investigation examined 15 statistical measures, eight for the HFM waveforms and seven for the FSK waveforms. The appendix defines the statistical measures in detail. Table 2 summarizes them. Measures are defined for threshold crossings through a peak for one beam or for clusters as a whole. There are two types of measure: shape and amplitude statistics. Shape statistics depend on threshold crossing time order. Amplitude statistics do not.

Both sea data and synthetic Gaussian random noise were used in this analysis. Synthetic data provide a basis for explaining the real data, and for testing the sensitivity of the statistics to the processing method used.

The processed sea data were separated into three categories. They were the direct blast, bathymetric returns, and ambient noise. Direct blast includes the direct blast arrival itself and the high SNR reverberation tail that follows it. These data were identified and discarded since this region was not of interest. The bathymetric region was identified by solving the bistatic range equation. Each threshold crossing was examined to determine if it was correlated with a feature on the bathymetric map. Correlated features were assumed to be caused by bathymetry. If it could not be associated, it was assumed to be ambient noise. Ambient noise also may contain background reverberation.

The means and CDFs of statistical measures were compared using three basic measures. First, the normalized difference between the means was compared using:

$$d = \frac{\bar{x}_1 - \bar{x}_2}{\sqrt{(\sigma_1^2 + \sigma_2^2)/2}} \tag{2}$$

The number of samples used to compute both means was large. Therefore, the normalized difference is an approximate measure of the separation of the means in units of the average standard deviation. The second measure was the Student's T statistic:

$$T = \frac{\bar{x}_1 - \bar{x}_2}{\sqrt{\frac{\sigma_1^2}{N_1} + \frac{\sigma_2^2}{N_2}}} \tag{3}$$

This is a measure of the standard error between the two means. T, N_1, N_2 are often used to compute the statistical significance between the means. For large underlying values of N_1 and N_2 in this work, values of $T \geq 3$ shows that the means are significantly different.

A third measure of the separation between two CDFs is the Kolmogorov-Smirnov static K-S. K-S is simply the largest difference between any two CDF for the same statistical measure at any value of that measure. K-S is therefore a number between 0 and 1. This is a well-known test of significance for comparing two CDFs based on K-S. Since the number of samples in each CDF estimate is high, K-S is used only as an indication of the separation of the CDFs.

In this paper d and K-S are used to compare CDFs as they might be used in a statistical filter to separate two classes. The significance of d may be seen by considering the example of two normal distributions with unit standard deviation with means separated by d. Assume that the filter is designed to reject only 10% of the threshold crossings in the desired class. For d = 0.25, only 15% of the undesired class would be rejected. That is, the CDFs are too close. For this same case, K-S = 0.1. Based on considerations like this, CDF pairs for which d is less than 0.25 and K-S is less than 0.1 are considered similar.

Figure 5 illustrates the three measures used to compare CDFs. Part a shows three CDFs generated using synthetic noise with the detection threshold set at 6, 8, and 10 dB. The value of d comparing 6 to 10 dB is about twice that comparing 6 to 8 dB, yet the value of T is about 1/2. (Of course, even at 12.7, the significance of the difference is almost certain.) Part b shows a more typical case. Here the value of d that compares the 6 and 8 dB cases is not large, but the value of T suggests that the difference is real. There is only a probability of 0.004 that the underlying population means are the same. The value of d that compares 6 and 10 dB is twice as large, but T is only 1.4. The probability that the underlying population means are the same is 0.14. Thus, primarily because of the smaller number of samples in the 10 dB curve, there is some doubt about significance of the difference.

Figure 5 also illustrates the primary use of K-S to show differences in CDF shape for cases where d is small. In Part b, K-S is 0.12 for the comparison between the 6 and 10 dB CDFs. Since d is small, the K-S shows a different CDF shape. It is, of course, possible to compare the significance of the differences in the CDFs using the full Kolmogorov-Smirnov test. Here K-S is simply used to indicate a distance. For cases where the mean differences are larger, such as in Part a, the K-S comparison is not particularly useful.

3. Results

Results are presented in four parts. The first part reports the sensitivity of the statistics to measurement conditions. The second part compares ambient noise measures to the same measures made on synthetic noise. The third part considers the variation of statistical measures over time. Finally, the last part compares bathymetric returns to ambient noise.

The first result is a comparison of the CDFs as a function of the detection threshold. This consists of 15 plots like the one shown in Figure 6a for SRT CDFs for 6 and 8 dB thresholds. This series of plots is summarized in the bar graphs of parts b and c. Here, the bars have been truncated at 10. Where this has been done, the value of the truncated bar is printed at the top of the bar. This presentation format will be used throughout.

Figure 6 shows that the normalized separation (d) for statistical measures is not large. It is usually less than one sigma, and sometimes much less. For the HFM results, SSkew and IF appear to have almost identical means. Because of the number of samples used in calculating the CDFs, there is a high level of significance in the difference. Examination of the CDFs suggests that this is mainly a displacement in the means, with the shape of the CDF not much altered. Remaining work was done for a threshold of 8 dB.

The grouping of similar waveforms before computing statistics had a possible effect on results. The results shown above are consolidated by waveform type. To study the effect of grouping, the statistics of the measures for synthetic noise with the waveforms kept

separate were computed. When HFM results were examined by waveform, SRT and ASD showed some sensitivity. Statistical significance was high, but d was less than 0.3. FSK showed little sensitivity. Waveforms are grouped by type for the remainder of the analysis.

The next major result was a comparison of ambient noise results with synthetic results. The results are summarized in Figure 7. The synthetic noise did an excellent job of matching the ambient noise results in that values of d are small. In several cases, the value of T is small, suggesting there is no difference. Synthetic data appear to explain at least the coarse features of the statistical measures as applied to ambient noise.

The stationarity of statistical measures is of interest. This analysis compared the CDFs for ambient noise for two 2-hour periods separated by two hours. Figure 8 shows the comparison. Because values of d are usually small, the value scale maximum has been changed. Again, Student's T shows that the small changes are real. The K-S statistic was always ≤ 0.01 for HFM measures AKurT, CD, and IF. Also, it was ≤ 0.01 for FSK measures AkurF, AkurT, and SRF.

A case for stationarity cannot be made from the results in Figure 8. Still, the changes are small and the CDFs are similar. Compared to commonly observed fluctuations in ambient noise power, these fluctuations are small. Techniques that adapt to temporal fluctuations in the CDF may prove useful in building a filter that exploits statistics.

The last major result is a comparison of echos from bathymetric features with ambient noise as shown in Figure 9. Again, values of d are mostly small. However, d and Student's T do not tell the whole story here because the standard deviation of the CDFs is changing. In previous results, the standard deviation has been nearly constant, and d and T have been good measures without K-S.

Figure 10 shows an additional comparison between CDFs for ambient and bathymetric noise. When the means are the same, larger values of K-S indicate differences in CDF shape or standard deviation. Part a provides an example of this. Part b shows K-S for comparisons of ambient and bathymetric CDFs. Part b also shows results comparing K-S values for the two ambient noise segments. The two sets of data show that the K-S values between bathymetry and noise are large compared to K-S values caused by temporal variation.

4. Discussion

Because this analysis is based on a limited data set, these results may not represent the ocean at large. With this reservation, the results support several conclusions:

Ambient noise behaves very much like synthetic noise. For a given detection threshold, differences between CDFs for synthetic and ambient noise are small. For the synthetic data, at least, statistical measures are only slightly sensitive to waveform. Within a

waveform type, waveforms that differ in parameters may be grouped for statistical filtering purposes.

Sea data results for ambient noise are slightly non-stationary. The differences in the CDFs for the two time segments are small. Signal processing algorithms have dealt with larger degrees of non-stationarity successfully.

The comparison of bathymetric with ambient noise CDFs shows significant differences. This has several consequences.

First, it is possible to separate ambient noise from bathymetric returns by statistics. However, this study has not shown that bathymetric returns are close to stationary in time. These returns may be dependent on the details of the bathymetry and the active sonar geometry employed. If bathymetric returns are not too unstationary, it may be possible to construct an area map that will characterize the CDFs. This analysis took the first steps toward doing this for one area.

Without *a priori* information about statistics for bathymetric returns for a shallow water area, these returns will simply complicate the statistical separation of signal and noise returns. Bathymetric returns will mix with ambient noise for an area in an unknown way. The performance of a statistical filter used to separate two classes depends on the separation of the CDFs. If one class, the noise, is ambient noise plus unknown bathymetry, the CDF for this combined class will have an uncertain CDF. This will increase the statistical difference between CDFs required to separate combined noise from other classes of objects (signals). For cases like this, large CDF separations will be required, and adaptive methods may be appropriate.

5. Appendix - Definition of the Statistical Measures

This investigation used 15 statistical measures, eight for the HFM waveforms and seven for the FSK waveforms. The HFM statistics are defined as follows. Let x(i) be the i^{th} matched filter output time sample. Let y(i) be the magnitude of x(i). Furthermore, assume that there is a local peak at i = 0.

The Spikiness Ratio in Time (SRT) is given by:

$$SRT = \frac{\frac{1}{33}\sum_{i=-16}^{16} y(i)}{\frac{1}{3}\sum_{i=-1}^{1} y(i)}. \qquad (4)$$

Other statistics are defined by moments. The amplitude moments do not consider time

order. Shape moments do. The amplitude moments are:

$$m_1 = \frac{1}{33}\sum_{i=-16}^{16} y(i) \tag{5}$$

and for n $\geq$ 2:

$$m_n = \frac{1}{33}\sum_{i=-16}^{16} (y(i) - m_1)^n. \tag{6}$$

The shape moments are given by:

$$ms_1 = \frac{1}{33}\sum_{i=-16}^{16} i\ y(i), \tag{7}$$

and for n $\geq$ 2:

$$ms_n = \frac{1}{33}\sum_{i=-16}^{16} (i\ y(i) - ms_1)^n. \tag{8}$$

The Amplitude Standard Deviation (ASD) is given by:

$$ASD = \frac{\sqrt{m_2}}{y(0)}, \tag{9}$$

the Amplitude Kurtosis in Time (AKurT) by:

$$AKurT = \frac{m_4}{m_2^{\,2}}, \tag{10}$$

the Shape Kurtosis (Skur) by:

$$Skur = \frac{ms_4}{ms_2^{\,2}}, \text{ and} \tag{11}$$

the Shape Skew (SSkew) by:

$$SSkew = \frac{ms_3}{ms_2^{\frac{3}{2}}}. \tag{12}$$

The Instantaneous Frequency (IF) is given by:

$$IF = \frac{d}{dt}\tan^{-1}\left(\frac{x(t)_{imag}}{x(t)_{real}}\right)_{t=0}. \tag{13}$$

Here imag indicates the imaginary part, and real indicates the real part.

The Threshold Crossing Width (TXW) is the time span covered by consecutive threshold crossings around the peak of interest. The sequence is defined by the first peak to exceed the threshold and stopped by the second peak to fall below it.

The last HFM statistic is a cluster statistic. The other statistics are based on a sequence of threshold crossings for a single beam. Here, the clustering process first indicates a set of threshold crossings, {i,k}, in delay time (i) and beam (k) that belong to a cluster. Let s(i,k) be the SNR for y(i,k). The Cluster Duration (CD) is defined by:

$$CD = 2\left(\frac{\sum_{\{i,k\}} (t_{i,k}-\bar{t})^2 s(i,k)}{\sum_{\{i,k\}} s(i,k)}\right)^{\frac{1}{2}}, \tag{14}$$

with:

$$\bar{t} = \frac{\sum_{\{i,k\}} t_{i,k} s(i,k)}{\sum_{\{i,k\}} s(i,k)}. \tag{15}$$

FSK statistics are defined similarly. Let z(i,j) be the i^{th} time series amplitude estimate output from a matched filter for the j^{th} Doppler cell. We assume a local peak at i = 0 and j = 0.

The Spikiness Ratio in Time (SRT) is given by:

$$SRT = \frac{\frac{1}{23}\sum_{i=-11}^{11} z(i,0)}{\frac{1}{3}\sum_{i=-1}^{1} z(i,0)}, \text{ and} \tag{16}$$

the Spikiness Ratio in Frequency (SRF) is given by:

$$SRF = \frac{\frac{1}{29}\sum_{j=-14}^{14} z(0,j)}{\frac{1}{3}\sum_{j=-1}^{1} z(0,j)}. \tag{17}$$

Here the summation limits have been dictated by the number of delay cells and number of Dopplers processed in an epoch.

Other statistics are defined by moments. In the time dimension, the amplitude moments are:

$$mt_1 = \frac{1}{23}\sum_{i=-11}^{11} z(i,0), \tag{18}$$

and

$$mt_n = \frac{1}{23}\sum_{i=-11}^{11} (z(i,0) - mt_1)^n. \tag{19}$$

Likewise, in the frequency dimension they are:

$$mf_1 = \frac{1}{29}\sum_{j=-14}^{14} z(0,j), \tag{20}$$

and for $n \geq 2$:

$$mf_n = \frac{1}{29}\sum_{j=-14}^{14} (z(0,j) - mf_1)^n. \tag{21}$$

The first shape moment in the time domain is given by:

$$mts_1 = \frac{1}{23}\sum_{i=-11}^{11} i\ z(i,0), \tag{22}$$

and in the frequency domain by:

$$mfs_1 = \frac{1}{29}\sum_{j=-14}^{14} j\ z(0,j). \tag{23}$$

The Amplitude Kurtosis in Time (AKurT) is given by:

$$AKurT = \frac{mt_4}{mt_2^{\,2}}, \tag{24}$$

the Amplitude Kurtosis in Frequency (AKurF) by:

$$AKurF = \frac{mf_4}{mf_2^{\,2}}. \tag{25}$$

The Threshold Delay Spread (TXS) is defined by:

$$TXS = \left(\frac{1}{23\,mt_1}\sum_{i=-11}^{11}\left(i - \frac{mts_1}{mt_1}\right)^2 z(i,0)\right)^{1/2}. \tag{26}$$

The Threshold Doppler Spread (DopSd) is defined by:

$$DopSd = \left(\frac{1}{29\,mf_1}\sum_{j=-14}^{14}\left(j - \frac{mfs_1}{mf_1}\right)^2 z(0,j)\right)^{1/2}. \tag{27}$$

Finally, the Cluster Duration (CD) is defined in terms of the cluster. Here, the clustering process first indicates a set of threshold crossings, {i,j,k}, in delay time, frequency, and beam that belong to a cluster. The Cluster Duration (CD) is defined by:

$$CD = 2\left(\frac{\sum_{\{i,j,k\}} (t_{i,j,k} - \bar{t})^2 s(i,j,k)}{\sum_{\{i,j,k\}} s(i,j,k)}\right)^{\frac{1}{2}}, \tag{28}$$

with:

$$\bar{t} = \frac{\sum_{\{i,j,k\}} t_{i,j,k} s(i,j,k)}{\sum_{\{i,j,k\}} s(i,j,k)}. \tag{29}$$

In the above equations, scale factors that produce units have been suppressed. Time units in the statistics are in seconds or Hertz as appropriate.

6. Acknowledgements

This work was sponsored by the Office of Naval Research.

Table 1. FSK Chip Masks

		WT1	WT2
Chip	duration (sec)	frequency (Hz)	frequency (Hz)
1	0.5	fo + 8	fo - 72
2	0.5	fo + 24	fo - 56
3	0.5	fo + 56	fo - 24
4	0.5	fo + 32	fo - 48
5	0.5	fo + 72	fo - 8
6	0.5	fo + 64	fo - 16
7	0.5	fo + 48	fo - 32
8	0.5	fo + 16	fo - 64
9	0.5	fo + 40	fo - 40

Table 2. Statistical Measures Used in the Analysis

Group	Measure	Code	domain	for
HFM	Spikiness Ratio in Time	SRT	time	one beam
	Amplitude Standard Deviation	ASD	time	one beam
	Amplitude Kurtosis in Time	AKurT	time	one beam
	Shape Kurtosis	Skur	time	one beam
	Shape Skew	SSkew	time	one beam
	Instantaneous Frequency	IF	phase	one beam
	Threshold Crossing Width	TXW	time	one beam
	Cluster Duration	CD	time	cluster
FSK	Spikiness Ratio in Time	SRT	time	one beam
	Spikiness Ratio in Frequency	SRF	freq	one beam
	Amplitude Kurtosis in Time	AKurT	time	one beam
	Amplitude Kurtosis in Frequency	AKurF	freq	one beam
	Threshold Delay Spread	TXS	time	one beam
	Threshold Doppler Spread	DopSd	freq	one beam
	Cluster Duration	CD	time & freq	cluster

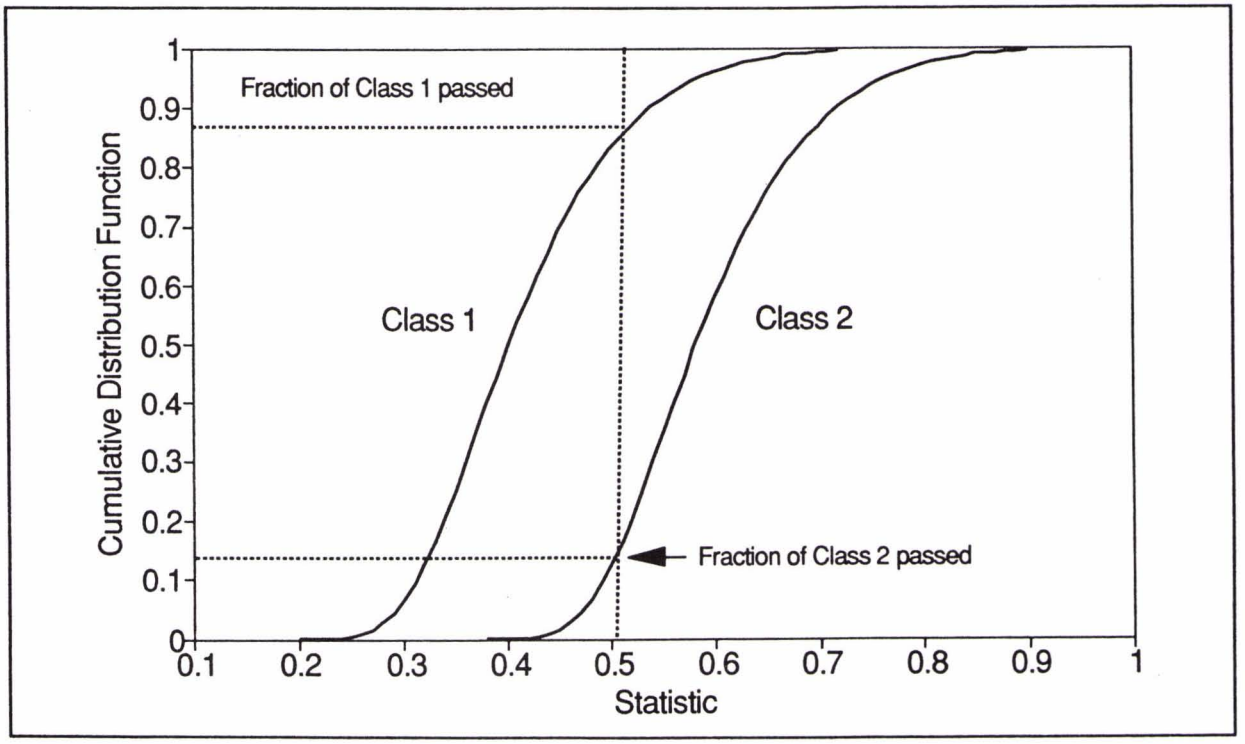

Figure 1. Statistical Separation into Two Classes

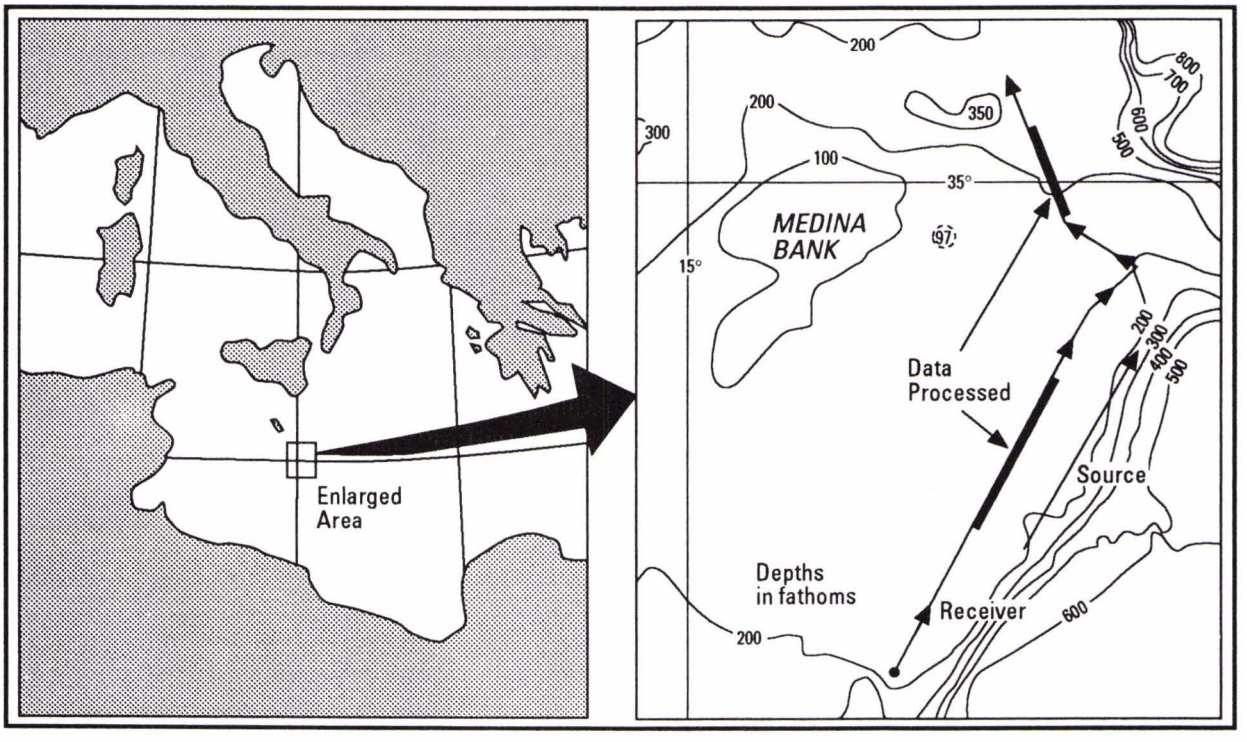

Figure 2. Test Area and Platform Tracks

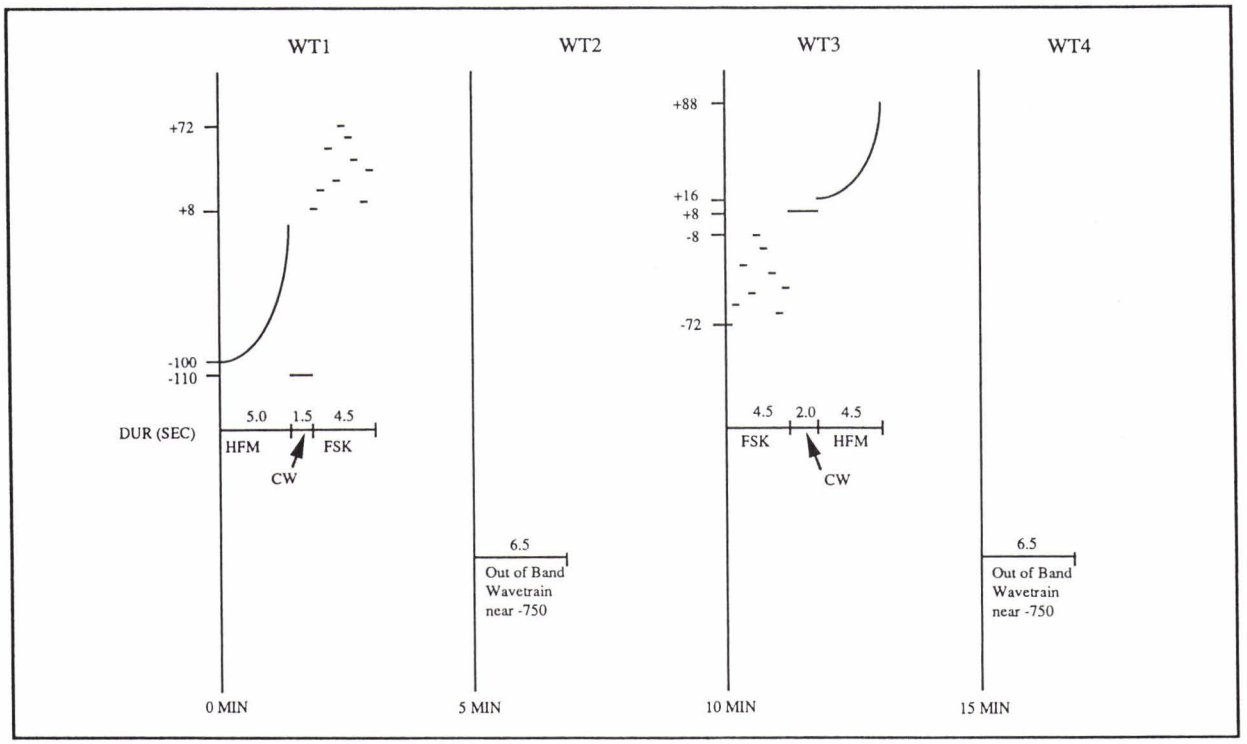

Figure 3. Waveforms and Transmission Schedule

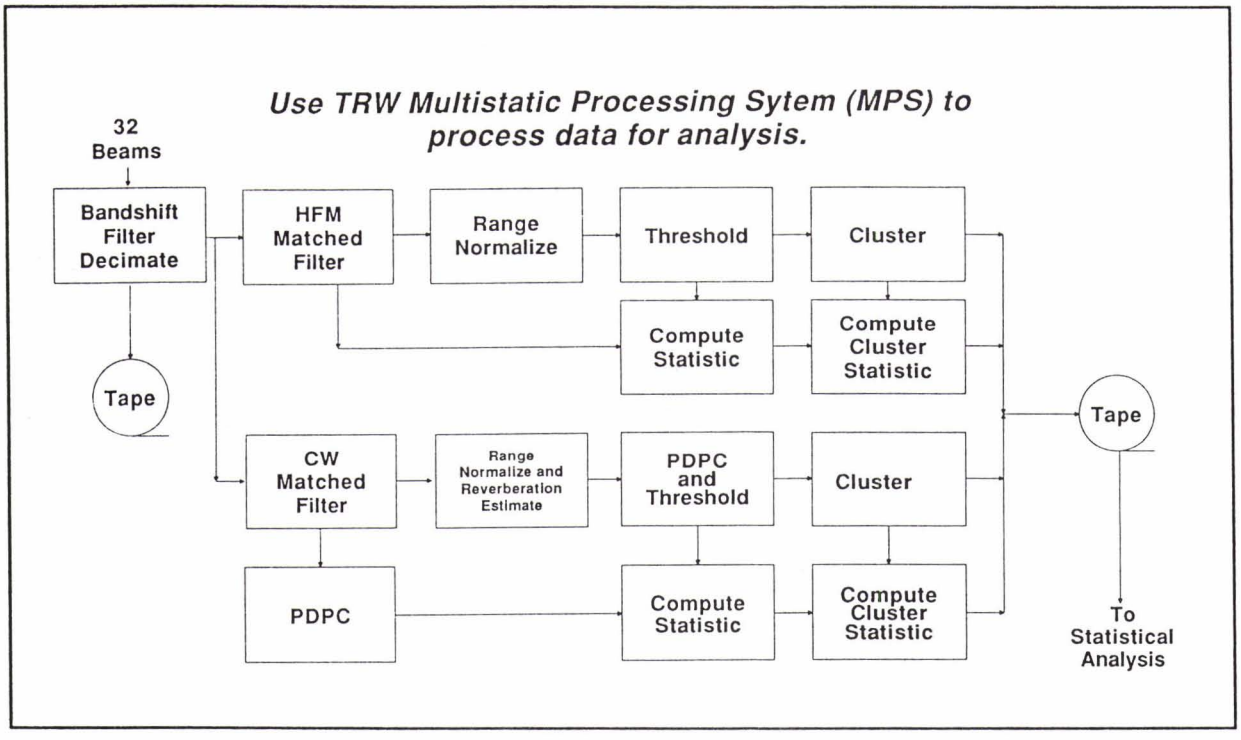

Figure 4. Data Processing Functional Flow

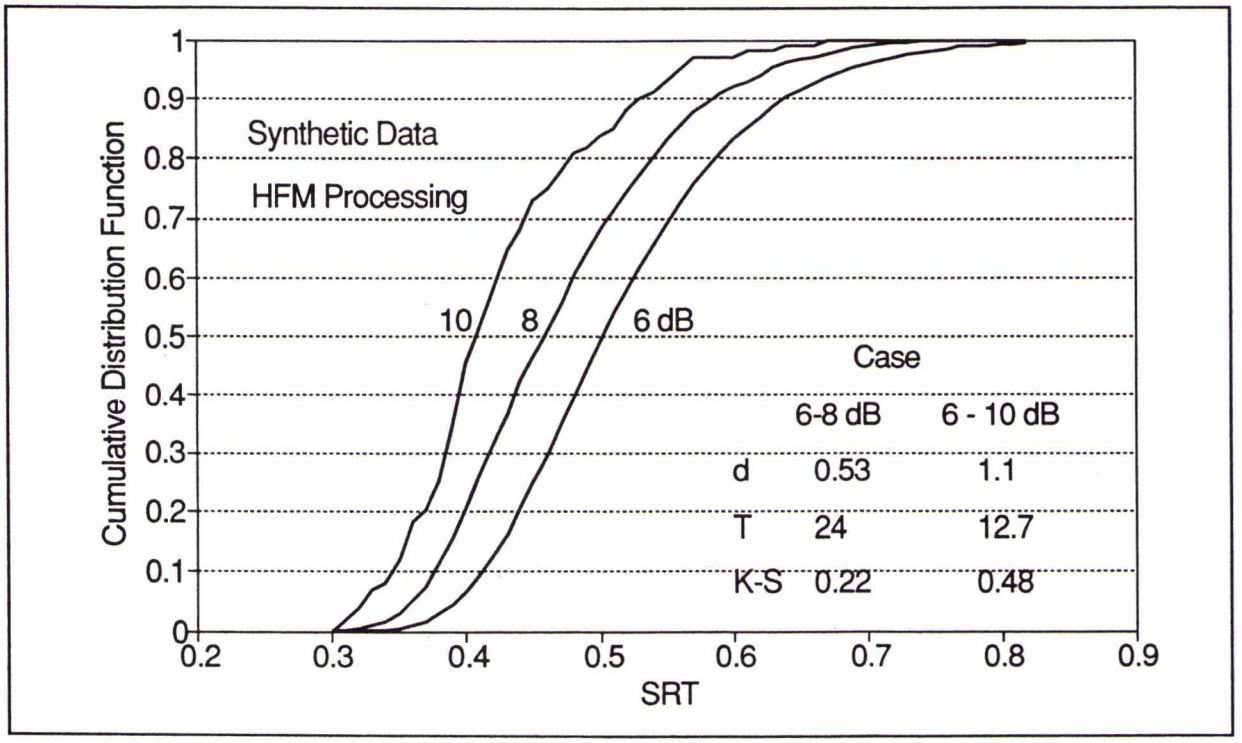

a. Example of CDFs with Large Mean Differences

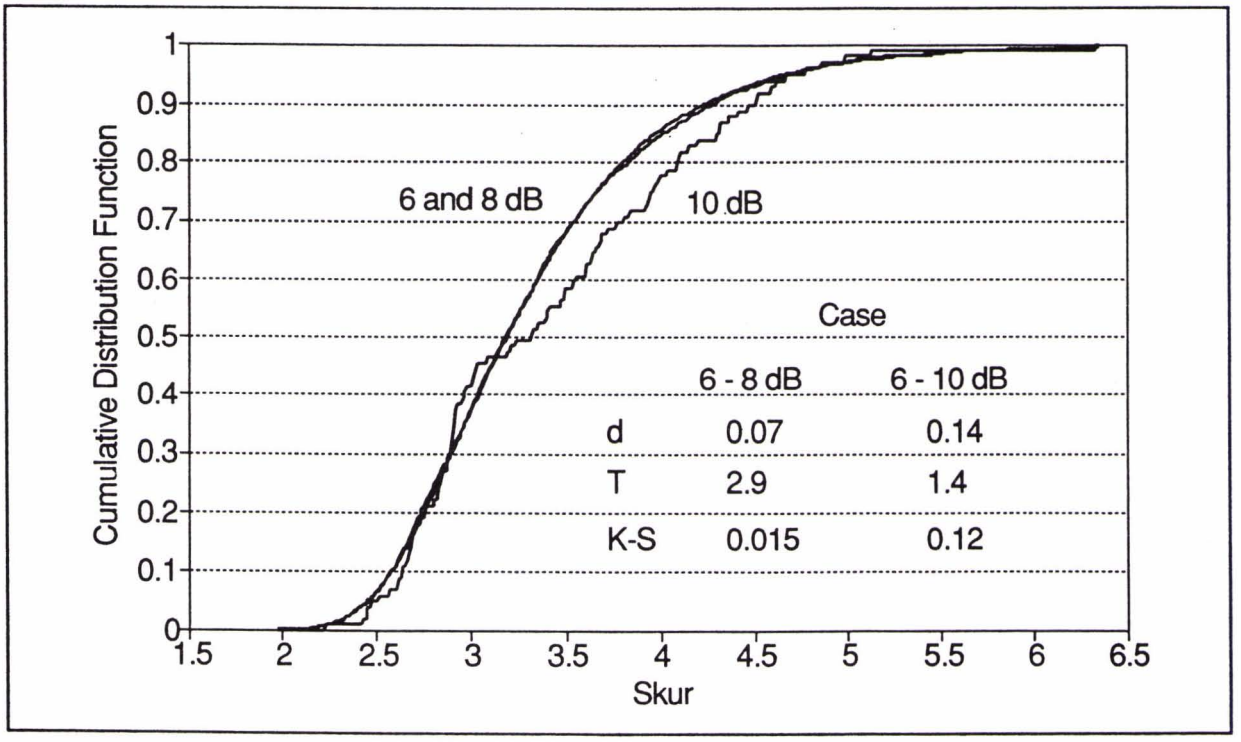

b. Example of CDFs with Small Mean Differences

Figure 5. Meaning of the Test Statistics

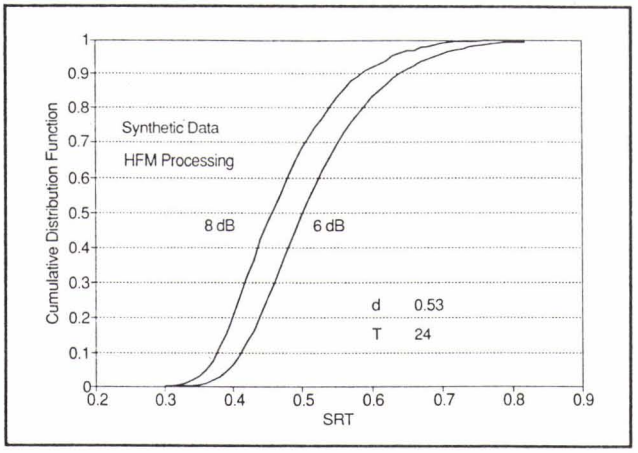

a. CDF Example

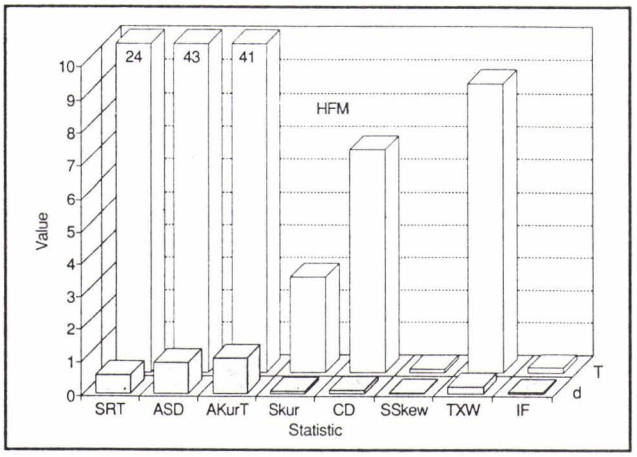

b. HFM Comparison

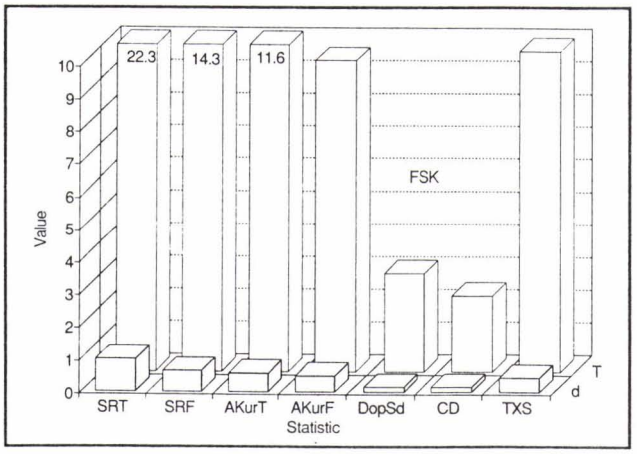

c. FSK Comparison

Figure 6. Sensitivity of the Tests to SNR Threshold

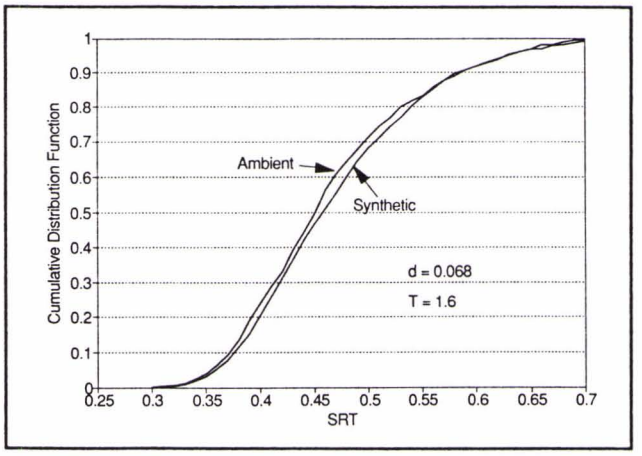

a. CDF Example

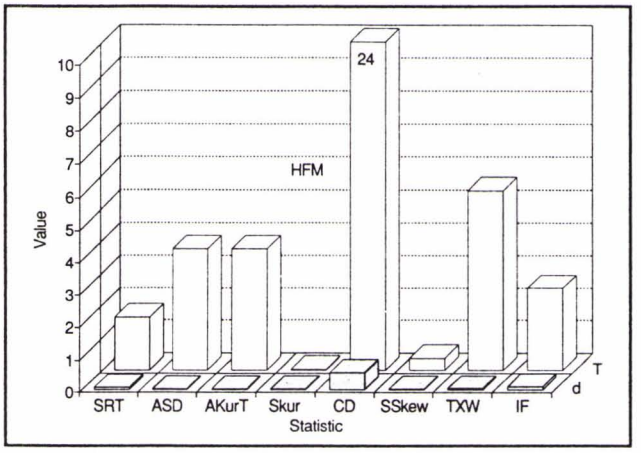

b. HFM Comparison

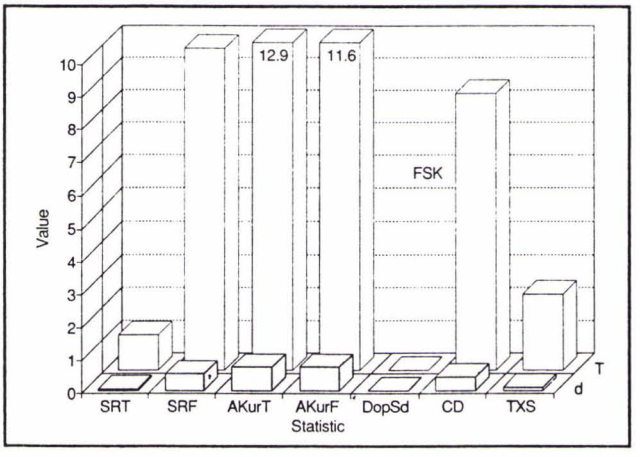

c. FSK Comparison

Figure 7. Comparison of Synthetic and Ambient Noise Results

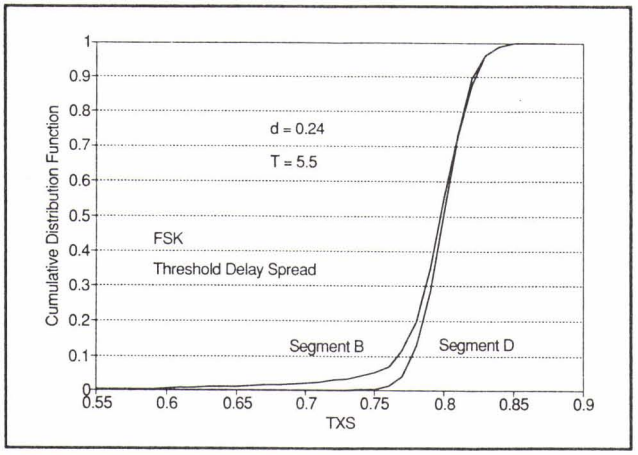

a. CDF Example

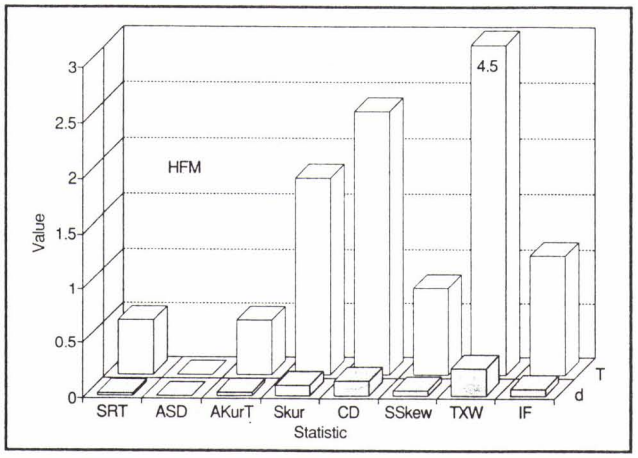

b. HFM Comparison

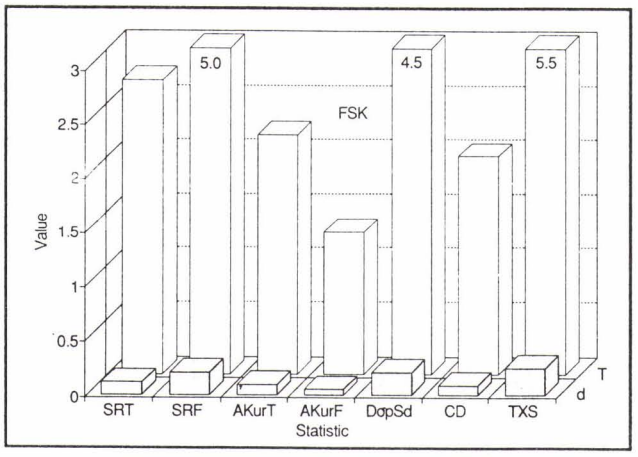

c. FSK Comparison

Figure 8. Variation of Ambient Noise Statistics with Time

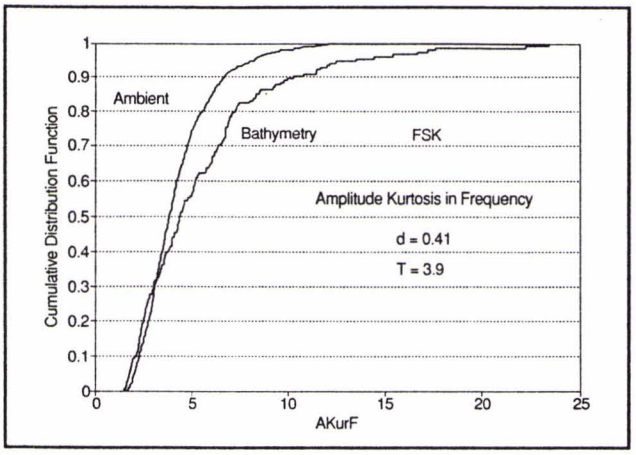

a. CDF Example

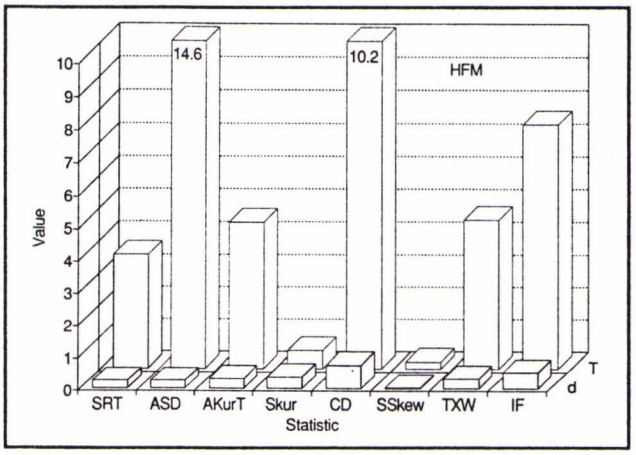

b. HFM Comparison

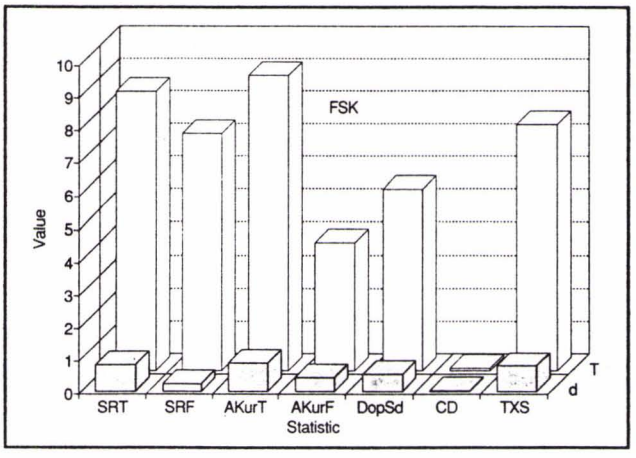

c. FSK Comparison

Figure 9. Comparison of Ambient Noise and Bathymetric Returns

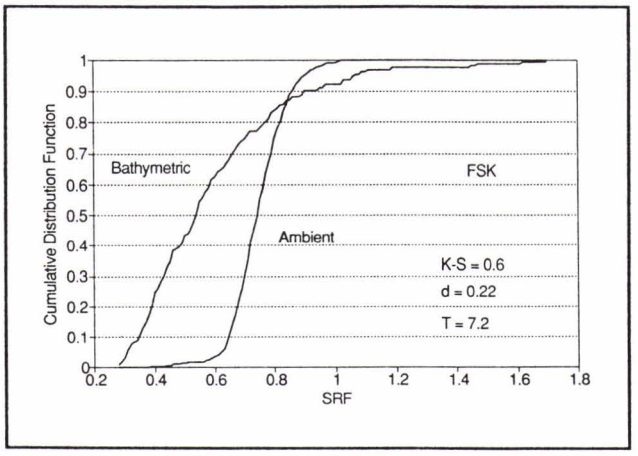

a. CDF Example

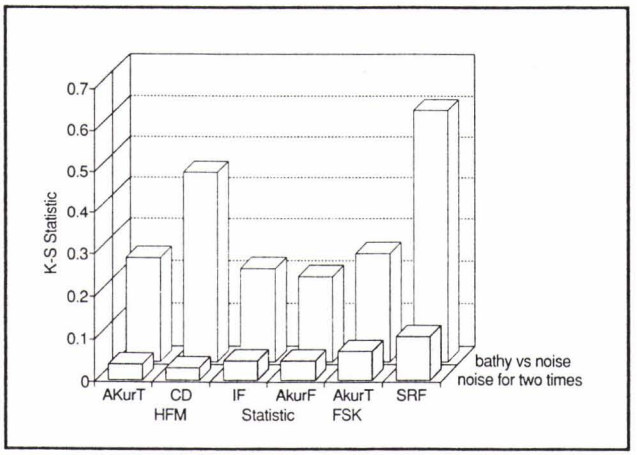

c. K–S Statistics Compared

Figure 10. CDFs for Ambient Noise and Bathymetric Returns